MECSOL Joinville 2017
April 26-28, 2017
Joinville, Santa Catarina, Brazil

INTERPRETRATION OF DENSITY-BASED TOPOLOGY OPTIMIZATION RESULTS BY MEANS OF A TOPOLOGICAL DATA STRUCTURE

Hugo B. S. Bruno
Department of Civil Engineering
PUC-Rio
hugobastos@id.uff.br

Guilherme C. G. Barros
Department of Civil Engineering
PUC-Rio
guilhermebarros@id.uff.br

Luiz F. Martha
Department of Civil Engineering
PUC-Rio
lfm@tecgraf.puc-rio.br

Ivan F. M. Menezes
Department of Mechanical Engineering
PUC-Rio
ivan@tecgraf.puc-rio.br

ABSTRACT

The results obtained with density-based topology optimization method are usually comprised of a discrete density field that represents the optimal material distribution within the structure. Although this technique leads to an optimal numerical solution, human intervention is often needed to obtain a practical design. One of the main steps towards obtaining the final design involves the computational modeling of the structure in order to perform further numerical simulations to verify the design criteria. This step may involve handwork and often reveals itself as a cumbersome and error-prone task. To circumvent this problem, several procedures are available in the literature concerning the geometrical interpretation of density-based results. However, none of them fully address the computational modeling i.e. geometric definition; attribute management; and discretization. This work proposes the use of the Half-Edge Topological Data Structure to automatically build 2D models from the interpreted geometric data. This data structure is particularly suitable since it is capable of handling complete planar subdivision, i.e., a subdivision of a two-dimensional space in which the entire space is filled with topological faces (no empty planar regions). Several numerical examples are present to demonstrate the efficiency and robustness of the proposed scheme.

Keywords: Topology Optimization, Density contours, Half-Edge

1. INTRODUCTION

Topology optimization address the problem of finding the best material distribution, within the design space, which optimizes a given performance measure (e.g.,the structural compliance) subject to a set of design constraints (e.g. stress constraints). This methodology can handle a wide set of constraints while still providing high-performance and low-cost designs, thus presenting itself as an attractive tool for industrial design purposes.

As a matter of fact, this technique has been widely employed in real-life structural applications including the optimization of aircraft wings [1], automotive components [2] and design of reinforced concrete structures [3]. However, as noted in [4], density-based topology optimization solutions are often considered as conceptual, given that a post-processing stage is needed to obtain a manufacturable design. This step usually involve handwork [5] and often reveals itself as a cumbersome and error-prone task.

To circumvent this problem, several procedures are available in the literature concerning the shape extraction of topology optimization results. For example, in [6], the authors propose an automated procedure which integrates the interpretation of density-based topology optimization results with the additive manufacturing technology, colloquially known as 3D printing. In such work, the density contours of the optimal result are obtained by interpolation of density nodal values, thus leading to tessellated surfaces which are directly outputted to suitable additive manufacturing file formats. Alternatively, in [7], representative cross-sections are used for reconstructing the 3D topology optimization results. Each cross section is interpreted as a two-dimensional result in which the interpolated density nodal values are appropriately fitted by splines. One of the main advantage of such approach is that it leads to a computer-aided design (CAD) model which may used for latter design stages as well as for additive manufacturing purpose. A common drawback inherent to such procedures, as noted in [6], is that interpreted results are no longer optimal and may also not comply with the given design criteria, thus slightly deteriorating the topology optimization solutions.

In order to assess such degradations, further numerical simulations must be performed, thus requiring the computational modeling of the final designs. To fulfill such requirement, this work proposes the use of the Half-Edge Topological Data Structure to automatically build models from the interpreted geometric data. In addition, to demonstrate the flexibility of such modeling, a linear elastic analysis of the interpreted results is carried out. A brief overview of each stage involved in the proposed approach is introduced throughout the text.

2. TOPOLOGY OPTIMIZATION

In the field of structural optimization, structural parameters are manipulated in order to render a performance measure its optima and satisfy a set of constraints. The performance measure, as well as the constraints, may be cost related or a structural response. Topology optimization is a branch of structural optimization in which the material distribution within a structure is optimized. The standard formulation of topology optimization is: find the material distribution that minimizes the compliance subject to a volume constraint, which is a bounded amount of material to distribute [8].

In the density-based topology optimization, the material distribution is modeled using a domain discretization. In this approach, the design variables are the density associated to each element within the discretization. The structural response, required by the optimization, is most commonly found using the finite element method, which also requires a domain discretization [9]. In this case, the domain discretization is often the same for density interpolation and finite element analysis.

Theoretically speaking, the density may only be zero or one, which means there is material in this element of the discretization or not. However, this problem would be discrete and not suitable for most optimization method available. In order to overcome this hurdle, a continuum density between

zero and one is allowed and the solution is subsequently penalized so that the final solution tends to one or zero. This approach is known as Solid Isotropic Material with Penalization (SIMP) [10].

This formulation provides interesting results and has been widely used in literature. However, its results consist in a collection of density values through the domain, which may give the impression of topology but, in fact, does not possess a single piece of topological information. For instance, it is illustrated in Figure 1 the result of the benchmark MBB-beam problem for density-based topology optimization, in order to illustrate the typical result obtained from this technique.

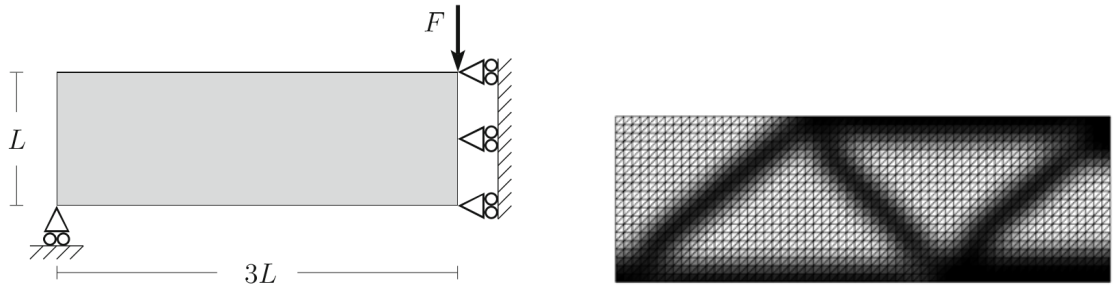

(a) MBB-beam problem setting [11] (b) Density-based topology optimization result

Figure 1. Typical density-based topology optimization result

In addition, regarding practical application, the structural safeness and serviceability must be verified. Unfortunately, the output density field of a density-based topology optimization does not provide the wherewithal for further analyses.Therefore, in order to assess the suitability of the design provided by the density-based topology optimization, an interpretation procedure, such as the one presented herein, is fundamental. Furthermore, some examples show that topology optimization may not suffice, requiring modifications in order to determine the final design. Such modifications might be performed manually or by means of a shape optimization, which is preferable; both approaches can profit greatly from the interpreted model.

3. DENSITY CONTOURS

Several approaches towards recovering geometric information from density-based topology optimization results are available in the literature. According to [7], such approaches may be divided in three main categories: image interpretation approach [12], geometric reconstructing approach [13] and density contour approach [14]. The image interpretation approach relies on computer vision technologies and image processing techniques. Specifically, the *"gray"* density results are initially converted to black-and-white images for which the boundary may be obtained by suitable image processing algorithms. In the geometric reconstruction approach, the boundaries are represented by mathematical geometric reconstruction routines based on computer-aided design (CAD) techniques. The density contour approach is based on contour plotting techniques of continuous scalar fields. Such techniques rely on the interpolation of nodal values in order to identify the iso-contours.

In this work, we employ the density contour approach in order to obtain a reliable and automated process towards identifying piecewise linear representations of the structure's boundaries. Likewise in stress recovery techniques for FEM, the first stage of this process is to obtain density values ρ_i at each of the mesh's nodes. This step is usually performed by suitable extrapolation of each element's density values $\rho^{(i)}$ to its neighboring nodes. In the simplest case, i.e. each element has a constant density value, this process reduces to a simple averaging of the density values of the elements connected to a given node. A simple example of such process is depicted in Figure 2.

With the nodal values in hand, it is then straightforward to identify the discrete points of a given contour line by simple linear interpolation. In addition, if the elements' edges are traversed in a ori-

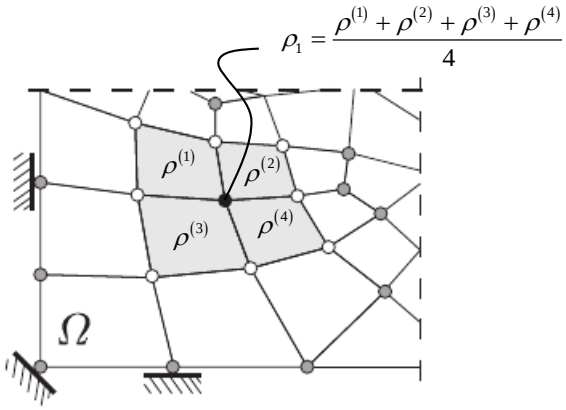

Figure 2. Interelement averaging

ented fashion, the straight line segments of the contour may be readily obtained by simply connecting the interpolated points. Figure 3 depicts the procedure for a single element(in this case the element's edges are traversed in a counter clock-wise orientation).

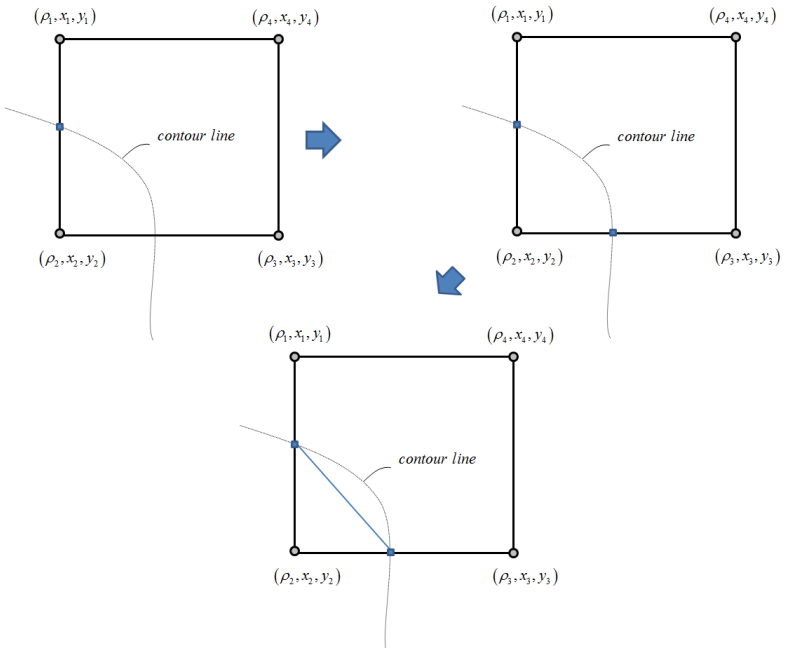

Figure 3. Nodal interpolation

After performing such procedure for every element of the mesh, the real contour line is roughly sketchted by a sequence of connected straight lines segments. For instance, Figure 4 depicts the density contour plot for the topology optimization result of the MBB beam problem, while Figure 5 illustrates the approximated contour line for a density level of 0.35.

Although the boundaries' geometry has been be roughly sketched, the data obtained by such procedure is only enough for visualization purposes. As a matter of fact, such data is comprised of a list of disjoints straight line segments for which topology information can only be inferred by human visual interpretation. Therefore, the next stage consists of sending such list of segments to the half-edge data structure, which is able to automatically obtain such informations.

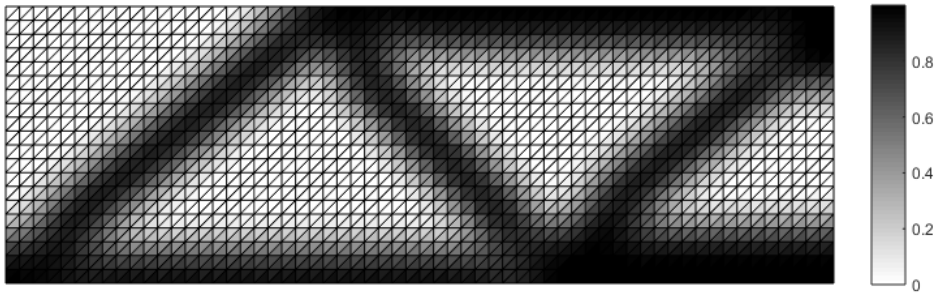

Figure 4. Density plot for the MBB problem

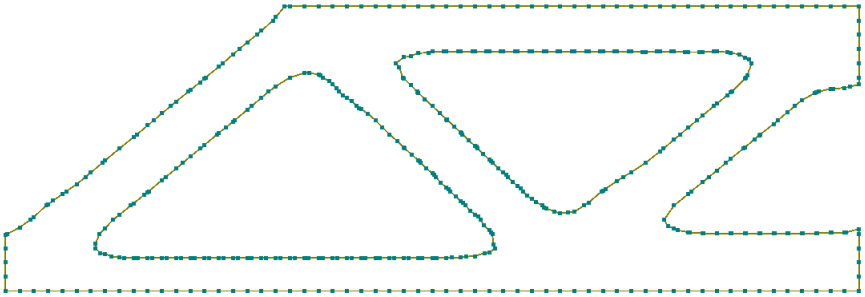

Figure 5. Interpretation for the MBB problem

4. HALF-EDGE

The half-edge topological data structure was first introduced by Mantyla [15] with the main purpose of introducing a topological data structure for solid modeling. Although the half-edge data structure has proved itself to be a powerful tool in handling, storing and saving solid models, it revealed to be only applicable for manifolds geometries. In order to overcome this hurdle, different topological data structures have been proposed [16, 17, 18, 19, 20].

In three dimensions, 2-manifold means that a small sphere intersecting the solid may only be divided into two subsets. Even though half-edge has drawbacks in representing three dimensional solids, it can still be handful for two-dimensional planar models. In other words, the half-edge data structure is capable of representing planar subdivisions in which a small circle is divided into many subsets.

This data structure concentrates a great amount of data within the topological entity called half-edge, which is an oriented edge within a loop of a face. Therefore, most topological queries are performed using information stored in such entity. In summary, the half-edge data structure has the following topological entities: vertices; edges; half-edges; faces; loops; and solids. The linkage of these entities is, thus, crucial to the consistency of the topological data.

In order to consistently build such topological model, the half-edge data structure is manipulated by means of the so-called Euler operators [21], which are appropriately designed as to satisfy the Euler-Poincaré formula:

$$V - E + F - (L - F) - 2(S - G) = 0 \tag{1}$$

in which V is the number of vertices; E is the number of edges; F is the number of faces; L is the number of loops; S is the number of solids; and G is the number of genus. Table 1 demonstrates some of the possible Euler operators and the changes they make upon the model.

Table 1. Some Euler operators

Operator Name	Meaning	V	E	F	L	S	G
MVFS	Make a vertex, a face and a solid	+1		+1	+1	+1	
MVR	Make a vertex and a ring (loop)	+1			+1		
MEV	Make an edge and a vertex	+1	+1				
MEKL	Make an edge and kill a loop		+1		-1		
MEF	Make an edge and a face		+1	+1	+1		

Following this idea, the model's constructive procedure relies on progressively calling the proper Euler operators according the desired changes to the model. An example of such construction is depicted in Figure 6.

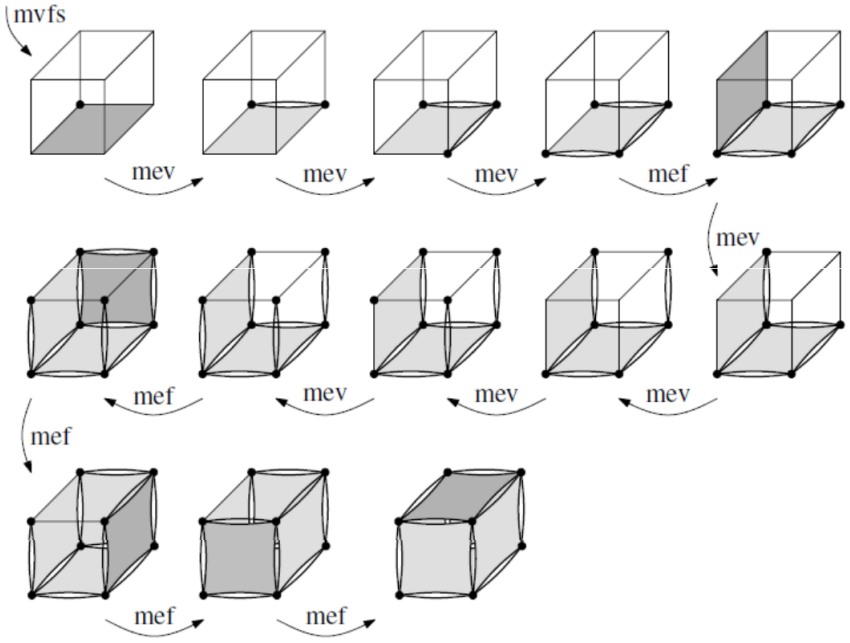

Figure 6. Constructive procedure of a simple parallelogram

This topological data structure plays a crucial role in the framework presented in this work for the interpretation of topology optimization results. Since the density contour algorithm outputs a list of disjoint line segments, the half-edge data structure is used to bring these line segments together into a consistent model.

When the first segment is inserted, the MVFS operator is called to initialize the model. For the subsequent segments, a geometrical search must be carried out in order to locate coincident vertices to use MEV or MEF operator. The decision between MEV and MEF depends on whether one or both vertices of a segment exist in the model . When no vertex is found the operation is performed by initially calling MVR and subsequently MEV. It is worth noting that an auxiliary geometric data structure, the R-Tree [22], is used to speed up such geometric queries.

Once all the line segments have been inserted into the half-edge data structure, the model possess all topological information needed for the interpretation. Specifically, the geometry of the internal loops (holes), and the outer loop (boundary), are properly arranged in lists of coordinates oriented counterclockwise. This way, such lists may be readily outputted for the next stage where the piecewise linear boundaries will be smoothed by means of a *B-spline* curve fitting procedure.

5. B-SPLINE CURVE FITTING

Curve fitting address the problem of finding a curve, or algebraic function, which has the best fit to a series of data points. This process may be carried out by either interpolation, where the data points are exactly fitted, or the so-called smoothing approach, which relies on minimizing a given error measure, usually the square deviation.

In the context of this work, the curve fitting stage is responsible for obtaining curves which smoothly represents a sequence of points $\mathbf{c}_i \ (i = 1 \dots r)$ of open/closed polygons obtained in the previous stage. In order to directly communicate with the CAD design, cubic B-splines are chosen as the fitting curves. Furthermore, given the low accuracy due to the linear interpolation of the density nodal values, the smoothing approach is considered superior for the purposes of this stage. In the following, we give a brief review on B-splines. Afterwards, the curve fitting problem is stated.

5.1 B-splines

A two-dimensional dth-degree *B-spline* curve may be defined as the following linear combination

$$\mathbf{s}(t) = \sum_{i=1}^{n} B_{i,d}(t)\,\mathbf{p}_i \tag{2}$$

where $\mathbf{p}_i = (x_i, y_i)$ are the control points and $B_{i,d}(t)$ are the so-called B-splines blending functions, given as

$$\begin{aligned} B_{i,0}(t) &= \begin{cases} 1, & \text{if } t \in [t_i, t_{i+1}) \\ 0, & \text{otherwise} \end{cases} \\ B_{i,d}(t) &= \frac{t - t_i}{t_{i+d} - t_i} B_{i,d-1}(t) + \frac{t_{i+1+d} - t}{t_{i+1+d} - t_{i+1}} B_{i+1,d-1}(t) \end{aligned} \tag{3}$$

in which $\left(t_j\right)_{j=1}^{n+d+1}$ are the elements of a sequence of non-decreasing real numbers $\mathbf{t}$ called the knot vector, this is

$$\mathbf{t} = \left\{t_1, t_2, \cdots, t_{n+d+1}\right\}, \quad t_i \leq t_{i+1} \tag{4}$$

A *B-spline* may also be define as a piecewise polynomial curve of the form

$$\mathbf{s}(t) = \begin{cases} \mathbf{f}_{d+1}(t, \mathbf{p}_1, \cdots, \mathbf{p}_{1+d}) & t \in [t_{d+1}, t_{d+2}) \\ \mathbf{f}_{d+2}(t, \mathbf{p}_2, \cdots, \mathbf{p}_{2+d}) & t \in [t_{d+2}, t_{d+3}) \\ \vdots & \vdots \\ \mathbf{f}_n(t, \mathbf{p}_{n-d}, \cdots, \mathbf{p}_n) & t \in [t_n, t_{n+1}] \end{cases} \tag{5}$$

where the dth-degree polynomials $\mathbf{f}_i(t, \mathbf{p}_i, \cdots, \mathbf{p}_{i+d})$ are given by the following recurrence relation

$$\begin{aligned} f_{i,0}(t) &= \mathbf{p}_i \\ f_{i,d-r+1}(t) &= \frac{t_{i+r} - t}{t_{i+r} - t_i} f_{i-1,d-r}(t) + \frac{t - t_i}{t_{i+r} - t_i} f_{i,d-r}(t) \end{aligned} \tag{6}$$

for $i = d - r + 1, \dots, n$ and $r = d, d-1, \dots, 1$.

This piecewise polynomial feature ensures that the B-spline curve is $\mathscr{C}^{\infty}$ continuous inside each knot interval. In addition, the smoothness at the joints $\left(t_j\right)_{j=d+2}^{n}$ results from the following theorem [**?**]:

Theorem 1. *Suppose that the number t_{i+1} occurs m times among the knots $\left(t_j\right)_{j=1-i1}^{m+d}$ with m some integer bounded by $1 \leq m \leq d+1$, i.e.*

$$t_i < t_{i+1} = \ldots = t_{i+m} < t_{i+m+1} \tag{7}$$

then the spline $\mathbf{s}(t)$ has continuous derivatives up to order $d-m$ at the join t_i+1.

Therefore, if no knots are repeated along the knot vector, the *B-spline* curve is ensured to be, at least, $\mathscr{C}^{d-1}$ continuous over its entire parametric space. This flexibility allows for the construction of curves of almost any shape by appropriately choosing its degree, control points and knots. Hence, this feature makes the *B-spline* well-suited for curve fitting and data approximation purposes.

This flexibility also allows for the construction of smooth closed curves. A closed *d*th-degree *B-spline* is achieved by imposing $\mathscr{C}^{d-1}$ continuity between its initial and end parameters. Such conditions may be written as

$$\frac{d^k\mathbf{s}(t_s)}{dt^k} = \frac{d^k\mathbf{s}(t_e)}{dt^k} \quad k = (1,\ldots,d-1) \tag{8}$$

where t_s and t_e are the initial and end parameters.

In this work, the closed *B-splines* are defined over periodic knot vectors, given as

$$t_i = \frac{i-(d+1)}{(n+d)} \quad i = (1,\ldots,n+d+1) \tag{9}$$

Due to this choice, the continuity conditions of equation (1.7) is achieved by wrapping the first and last d control points, this is

$$\mathbf{p}_j = \mathbf{p}_{n-d+j} \quad j = (1,\ldots,d) \tag{10}$$

5.2 B-spline smoothing

The best fitting closed *dth*-degree *B-spline* $\mathbf{s}(t)$, with control points $\mathbf{p}_i$ $i = (1\ldots n)$, to a sequence of points $\mathbf{c}_i$ $(i = 1\ldots r)$ of a closed polygon is obtained by minimizing the square distance sum $\mathbf{f}$ between the curve and the data points, this is

$$\begin{cases} \min \quad \mathbf{f} = \sum\limits_{i=1}^{n} \left\|\mathbf{s}(u_i) - \mathbf{c}_i\right\|^2 \\ s.t. \quad \frac{d^k\mathbf{s}(t_s)}{dt^k} = \frac{d^k\mathbf{s}(t_e)}{dt^k} \end{cases} \tag{11}$$

where u_i $(i = 1\ldots n)$ is an arbitrary set of parameters on the interval $[t_s, t_e]$.

In this work we define such parameters by means of the chord length parametrization method [23], which gives

$$\begin{aligned} &u_1 = 0; \\ &u_i = \frac{\sum\limits_{j=2}^{i} \left\|\mathbf{c}_{j-1} - \mathbf{c}_j\right\|}{\sum\limits_{j=2}^{n} \left\|\mathbf{c}_{j-1} - \mathbf{c}_j\right\|}; \quad i = (2,\ldots,n-1) \\ &u_n = 1; \end{aligned} \tag{12}$$

The problem in equation 11 may be rewritten in the following matrix form

$$\begin{cases} \min & \mathbf{f} = \|\mathbf{Ap} - \mathbf{c}\|^2 \\ s.t. & \mathbf{Np} = 0 \end{cases} \tag{13}$$

where

$$A_{ij} = B_{j,d}(u_i) \quad \begin{matrix} i = (1,\ldots,r) \\ j = (1,\ldots,n) \end{matrix} \tag{14}$$

and

$$N_{ij} = \frac{d^{i-1}B_{j,d}(t_s)}{dt^{i-1}} - \frac{d^{i-1}B_{j,d}(t_e)}{dt^{i-1}} \quad \begin{matrix} i = (1,\ldots d) \\ j = (1,\ldots n) \end{matrix} \tag{15}$$

By expanding the squared norm of equation 13, the problem may be explicitly given as the following equality constrained quadratic program

$$\begin{cases} \min & \mathbf{f} = \mathbf{p}^T\mathbf{Qp} + \mathbf{b}^T\mathbf{p} \\ s.t. & \mathbf{Np} = 0 \end{cases} \tag{16}$$

for which the solution may be readily obtained by solving the following system of linear equations

$$\begin{bmatrix} \mathbf{Q} & \mathbf{N}^T \\ \mathbf{N} & 0 \end{bmatrix} \begin{bmatrix} \mathbf{p} \\ \lambda \end{bmatrix} = \begin{bmatrix} \mathbf{b} \\ \mathbf{0} \end{bmatrix} \tag{17}$$

where

$$\mathbf{Q} = \mathbf{A}^T\mathbf{A}; \quad \mathbf{b} = -2\mathbf{A}^T\mathbf{c} \tag{18}$$

and λ is a set of Lagrange multipliers.

The fitting of open *B-splines* is carried out in a similar fashion, except that the problem constraints are given as

$$s(t_s) = c_1; \quad s(t_e) = c_r \ ; \tag{19}$$

which ensures that the fitting *B-spline* interpolates the initial and end points of the open polygon.

In order to assess the efficacy of such scheme, the smoothing of leftmost internal loop, obtained in the previous stage, is carried out. The smoothing is performed by using cubic B-splines with 15 control points. Figure 7 shows the results of the smoothing procedure.

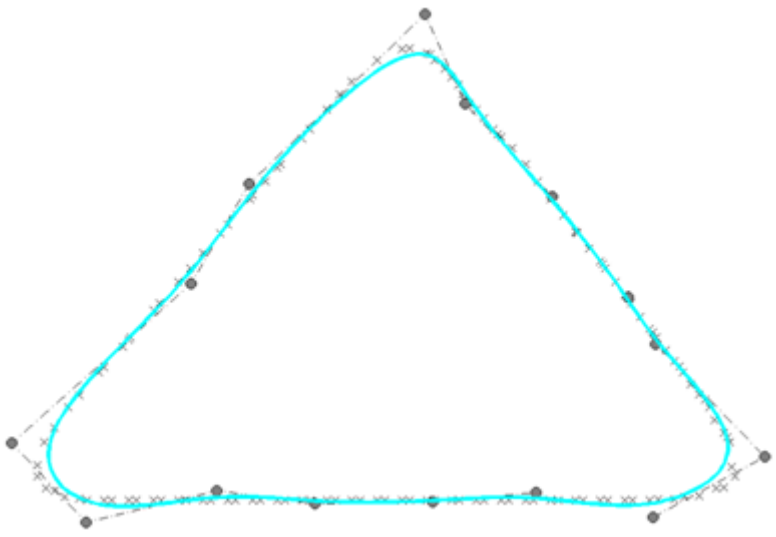

Figure 7. Smoothing result

6. RESULTS

To demonstrate the flexibility of such modeling, a linear elastic analysis of the interpreted result is carried out by the finite element method. It is worth mentioning that the main cumbersome steps towards this analysis, such as the mesh generation and boundary conditions enforcement, may be readily overcome by making use of the topological information provided by the half-edge data structure. Figure 8 and 9 illustrates, respectively, the results for the displacements and von Mises stresses for the final model.

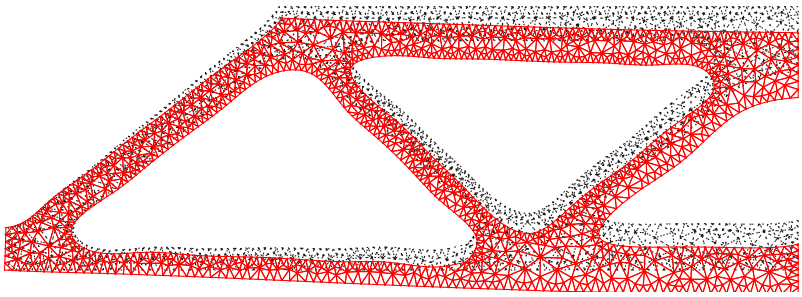

Figure 8. Displacement result

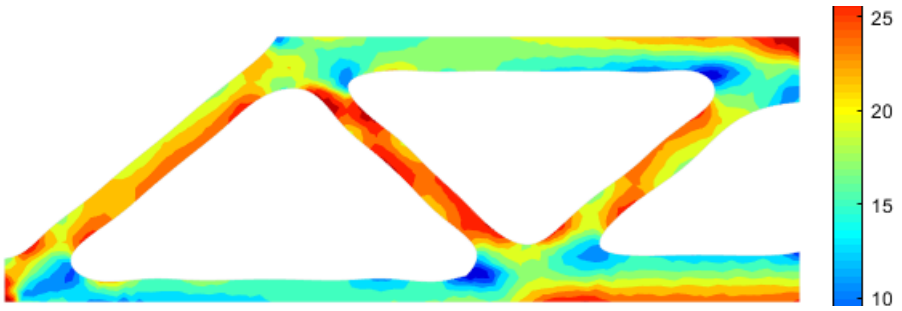

Figure 9. von Mises stress plot

7. CONCLUSIONS

This work has proposed an automated process towards the interpretation of density-based topology optimization results. In this framework, the half-edge plays a central role by appropriately providing topological information for the geometric interpreted result. Furthermore, the flexibility of the proposed modeling allows for a straightforward integration with the smoothing curve stage as well as with the analysis step. Also, the curve fitting by B-splines has proven to be an efficient and accurate procedure for obtaining smooth curves for a high-level description of the interpreted results. Another great asset of this choice is that a computer-aided design model of the interpreted result may be readily recovered, thus allowing for latter manual modification of the model.

It is important to point out that the proposed approach is also particular suitable for the integration of topology and shape optimization methods. This integration allows for a complete framework for the designing of high performance structures, which may be readily manufactured. Such integrated framework is currently underdevelopment by the authors.

REFERENCES

[1] Ananthasuresh, G. K. (2015). "Topology and Size Optimization of Modular Ribs in Aircraft Wings." In 11th World Congress on Structural and Multidisciplinary Optimisation, June, pages 1–6. Sydney.

[2] Yang, R. J. and Chahande, A. I. (1995). "Automotive applications of topology optimization." Structural optimization, 9(3):245–249. ISSN 1615-1488. doi:10.1007/BF01743977.

[3] Dombernowsky, P. and Sondergaard, A. (2009). "Three-dimensional topology optimisation in architectural and structural design of concrete structures." Proceedings of the International Association for Shell and Spatial Structures (IASS) Symposium 2009, Valencia, (October):1066–1077.

[4] Lazarov, B. S., Wang, F., and Sigmund, O. (2016). "Length scale and manufacturability in density-based topology optimization." Archive of Applied Mechanics, 86(1-2):189–218. ISSN 14320681. doi:10.1007/s00419-015-1106-4.

[5] Cappello, F. and Mancuso, A. (2003). "A genetic algorithm for combined topology and shape optimisations." Computer-Aided Design, 35(8):761–769. ISSN 00104485. doi:10.1016/S0010-4485(03)00007-1.

[6] Zegard, T. and Paulino, G. H. (2016). "Bridging topology optimization and additive manufacturing." Structural and Multidisciplinary Optimization, 53(1):175–192. ISSN 16151488. doi:10.1007/s00158-015-1274-4.

[7] Hsu, M.-H. and Hsu, Y.-L. (2005). "Interpreting three-dimensional structural topology optimization results." Computers & Structures, 83(4):327–337. ISSN 00457949. doi:10.1016/j.compstruc.2004.09.005.

[8] Bendsøe, M. P. and Sigmund, O. (2004). Topology optimization: theory, methods and applications. Springer, Berlin, 2nd edition. ISBN 978-3-642-07698-5. doi:10.1007/978-3-662-05086-6.

[9] Zienkiewicz, O. C., Taylor, R. L., and Zhu, J. Z. (2013). The Finite Element Method: Its Basis and Fundamentals. ISBN 9781856176330.

[10] Bendsøe, M. P. and Sigmund, O. (1999). "Material interpolation schemes in topology optimization." Archive of Applied Mechanics, 69(9-10):635–654. ISSN 0939-1533. doi:10.1007/s004190050248.

[11] Holmberg, E., Torstenfelt, B., and Klarbring, A. (2013). "Stress constrained topology optimization." Structural and Multidisciplinary Optimization, 48(1):33–47. ISSN 1615147X. doi:10.1007/s00158-012-0880-7.

[12] Lin, C. Y. and Chao, L. S. (2000). "Automated image interpretation for integrated topology and shape optimization." Structural and Multidisciplinary Optimization, 20(2):125–137. ISSN 1615147X. doi:10.1007/s001580050144.

[13] Chang, K. and Tang, P. (2001). "Integration of topology and shape optimizations for structural components." Structural and Multidisciplinary Optimization, 22(1):6. ISSN 1615-147X. doi:10.1007/PL00013282.

[14] Hsu, Y.-L., Hsu, M.-S., and Chen, C.-T. (2001). "Interpreting results from topology optimization using density contours." Computers & Structures, 79(10):1049–1058. ISSN 00457949. doi: 10.1016/S0045-7949(00)00194-2.

[15] Mantyla, M. (1988). An Introduction to Solid Modeling. Computer Science Press, Rockville, MD. ISBN 0-88175-108-1.

[16] Castelo, A., Lopes, H. C. V., and Tavares, G. (1992). "Handlebody representation for surfaces and Morse operators." pages 270–283.

[17] Cavalcanti, P. R., Carvalho, P. C. P., and Martha, L. F. (1997). "Non-manifold modelling: an approach based on spatial subdivision." Computer-Aided Design, 29(3):209–220. ISSN 00104485. doi:10.1016/S0010-4485(96)00066-8.

[18] Rossignac, J. and Cardoze, D. (1999). "Matchmaker: Manifold Breps for non-manifold r-sets." Proceedings of the fifth ACM symposium on . . . , pages 1–13. doi:10.1145/304012.304016.

[19] Weiler, K. J. (1985). "Edge-Based Data Structures for Solid Modeling in Curved-Surface Environments." doi:10.1109/MCG.1985.276271.

[20] Weiler, K. J. (1986). Topological Structures for Geometric Modeling. Phd thesis, Rensselaer Polytechnic Institute.

[21] Hoffmann, C. M. (1992). Geometric and Solid Modeling.

[22] Manolopoulos, Y., Nanopoulos, A., Papadopoulos, A., and Theodoridis, Y. (2006). R-Trees: Theory and Applications. ISBN 9788578110796. doi:10.1017/CBO9781107415324.004.

[23] Lee, E. (1989). "Choosing nodes in parametric curve interpolation." Computer-Aided Design, 21(6):363–370. ISSN 00104485. doi:10.1016/0010-4485(89)90003-1.

RESPONSIBILITY NOTICE

The following text, properly adapted to the number of authors, must be included in the last section of the paper:

The author(s) is (are) the only responsible for the printed material included in this paper.